ADVANCED FUNCTIONAL MATERIALS
www.afm-journal.de

CdS Quantum Dots Encapsulated in Chiral Nematic Mesoporous Silica: New Iridescent and Luminescent Materials

*Thanh-Dinh Nguyen, Wadood Y. Hamad, and Mark J. MacLachlan**

Simultaneous integration of light emission and iridescence into a semiconducting photonic material is attractive for the design of new optical devices. Here, a straightforward, one-pot approach for liquid crystal self-assembly of semiconductor quantum dots into cellulose nanocrystal-templated silica is developed. Through a careful balance of the intermolecular interactions between a lyotropic tetraalkoxysilane/cellulose nanocrystal dispersion and water-soluble polyacrylic acid/mercaptopropionic acid-stabilized CdS quantum dots, CdS/silica/nanocellulose composites that retain both chiral nematic order of the cellulose nanocrystals and emission of the quantum dots are successfully co-assembled. Subsequent removal of the cellulose template and organic stabilizers in the composites by controlled calcination generates new freestanding iridescent, luminescent chiral nematic mesoporous silica-encapsulated CdS films. The pores of these materials are accessible to analytes and, consequently, the CdS quantum dots undergo strong luminescence quenching when exposed to TNT solutions or vapor.

1. Introduction

Incorporation of functional dopants into photonic crystals could advance their optical responses useful for fabricating waveguide-based devices.[1] Semiconductor quantum dots (QDs) are an ideal light emitter with their tunable emissions that arise from quantum confinement effects.[2] Coupling of opto-electronic properties of the photonic structures with the semiconducting QDs could provide new materials with potential uses in fields of display technology, sensors, optical amplifiers, and lasers.[3] QD-based platforms have been widely developed for optical sensors,[4a,b,c] for example, in rapid, sensitive detection of nitroaromatic explosives via luminescence quenching.[4d,e]

Semiconducting photonic materials, such as inverse opals of CdSe QD-embedded TiO_2[5a] and CdTe QD-embedded ZnO,[5b] have been reported. The QD-deposited opal crystals were fabricated by loading QDs into the inverse opals that were prepared by template-assisted self-organization. The multi-step procedure to fabricate these materials is often difficult to achieve and expensive for production scale-up. Finding simple alternatives for fabricating these materials derived from renewable resources will be important for developing applications of the QD/photonic crystal composite materials.

Chiral biomacromolecules, such as polysaccharides, DNA, and proteins, are attractive natural templates for preparing solid-state materials as they have the possibility to transfer their chiral properties to the solid replicas.[6] Spindle-shaped cellulose nanocrystals (CNC) are renewable nanomaterials prepared by acid hydrolysis of bulk cellulose.[7] Above a critical concentration, aqueous dispersions of CNC can form a chiral nematic liquid crystal (LC) phase with a left-handed helical structure.[8] This material has been explored as an intriguing template for mesoporous solids.[9] Recently, we discovered that the chiral nematic LC phase of CNC can be used as a template to construct photonic silica and organosilica films.[10] After removal of CNC, mesoporous solid-state structures were obtained that acquire high surface area and long-range helical twist of the chiral nematic CNC. Helical pitch and porosity of these materials can be tailored by changing the concentration of silica-based sol–gel precursors, allowing for tunable photonic structures. Importantly, the materials are available as large, freestanding films.[11]

Metallic nanoparticles have been embedded within the chiral nematic mesoporous silica films, and it was shown that they exhibit circular dichroism (CD) signals that arise from dipolar coupling of the surface plasmon resonance.[12] Also, the metallic nanoparticles are accessible and show CD responses to adsorbed guests.[12b]

Previous efforts to incorporate hydrophobic trioctylphosphine oxide-capped CdSe/ZnS QDs into a cellulose derivative, cellulose triacetate, was achieved by Gray and co-workers.[13] Although the authors were able to disperse QDs within the polymer, the luminescent QD/cellulose triacetate composites showed neither chiral nematic organization nor porosity. We hypothesized that the luminescent semiconductor QDs may be incorporated into the chiral nematic porous structures templated by CNC to give new functional materials that combine

Dr. T.-D. Nguyen, Prof. M. J. MacLachlan
Department of Chemistry
University of British Columbia
2036 Main Mall, Vancouver
British Columbia, V6T 1Z1, Canada
E-mail: mmaclach@chem.ubc.ca
Dr. W. Y. Hamad
CelluForce, Inc.
3800 Wesbrook Mall, Vancouver, British Columbia, V6S 2L9, Canada

DOI: 10.1002/adfm.201302521

the iridescence of the chiral nematic phase and the luminescence of QDs. Moreover, it may be possible to incorporate QDs in a 1-step process, where QDs co-assemble with alkoxysilane and chiral nematic CNC template, and subsequent removal of the template. This could offer a simple procedure for integrating QDs into these structures.

Semiconductor QDs with hydrophilic surfaces are needed for co-assembling with the liquid crystalline cellulose in water. QDs prepared by popular hot injection methods are incompatible with the CNC mesophase because of their hydrophobic surfaces.[14a] Water solubility of the hydrophobic QDs could be improved by functionalizing with an alkoxysilane layer. However, the silica-coated core–shell QDs typically have large particle sizes,[14b] which are also expected to interfere with the chiral nematic order of CNC. To address this problem, aqueous preparations of the QD colloids passivated with appropriate amphiphilic stabilizers are necessary.

In this paper, we describe our work to self-assemble CdS QDs into chiral nematic CNC-templated silica, which generates freestanding iridescent, luminescent mesoporous silica-encapsulated CdS QD films after controlled calcination of CNC and other additives. The CdS QD colloids were prepared in water and subsequently treated with an amphiphilic polymer. The QD surface passivated with the amphiphilic stabilizers resulted in weak interactions between a lyotropic alkoxysilane/cellulose nanocrystal dispersion and water-soluble stabilized QDs, thus preserving both the chiral nematic order of CNC and intense emission of QDs in the films. The mesoporous semiconducting photonic CdS/silica materials undergo luminescence quenching when exposed to nitroaromatic compounds, suggesting their potential use in optical sensing applications.

2. Results and Discussion

In order to encapsulate the CdS QDs within a chiral nematic mesoporous silica through a one-pot self-assembly, we had to overcome several obstacles. Specifically, it was critical to prevent aggregation of the luminescent CdS nanoparticles during assembly and simultaneously to carefully control the reactant composition in order to maintain an iridescent chiral nematic structure. Water-soluble CdS QDs were initially prepared by hydrothermal reaction of a basic aqueous solution of cadmium acetate, thiourea, and 3-mercaptopropionic acid (MPA) at 100 °C for 24 h.[15] The resulting MPA-capped QDs dispersed in neutral or basic media, but they precipitated at pH ≤5 due to dissociation of the MPA capping molecules. Our previous report demonstrated that the chiral nematic pore order of the CNC-templated silica films is best preserved in acidic media at pH 2.4,[10a] so the MPA-capped CdS QDs are incompatible with this preparation. Polyacrylic acid (PAA) is an amphiphilic stabilizer that could adsorb on the MPA-capped CdS QDs to stabilize the colloidal dispersion.[16] Thus, the MPA-capped CdS QDs were coated with PAA in water to form PAA/MPA-stabilized QDs (see Experimental Section in Supporting Information). After coating with PAA, the colloidal QDs were stable in water over a wide range of pH ≈ 3–10 (Figure S1a, Supporting Information). The PAA/MPA-stabilized CdS QDs have an average particle size of 2.5 nm (using ImageJ software to obtain a particle size distribution from TEM analysis) and exhibit an absorption edge at 405 nm and an emission peak at 610 nm (λ_{exc} = 425 nm) corresponding to a band-gap energy of 2.87 eV (see details in Supporting Information). The resulting PAA/MPA-stabilized CdS QD aqueous solution with 5.14 mM concentration and pH ≈ 5 was used to yield iridescent, luminescent chiral nematic mesoporous CdS/silica materials in all of the preparations.

We initially prepared CdS/silica/CNC composites by co-assembling PAA/MPA-stabilized with $Si(OCH_3)_4$ and lyotropic CNC dispersion. The goal of preparing freestanding chiral nematic mesoporous CdS/silica films was to achieve a high loading of QDs and alkoxysilane to obtain highly emissive materials while retaining the visible photonic structure of the host.[10a,12b] Thus, the amount of the CdS QDs that could be added into the composites was limited to about 2.23 mM (1.4:100 Cd:Si) as higher concentrations led to substantial aggregation of the CdS QDs. However, we found that the composite films loaded with 2.23 mM QDs cracked substantially during preparation and the CdS QDs were not well dispersed. To overcome these problems, we added polyvinyl alcohol (PVA) to our preparations since PVA has been demonstrated to reduce cracking in pure CNC films.[17]

After these difficulties were overcome, a series of CdS/silica/CNC composites was prepared using $Si(OCH_3)_4$ as silica precursor, CNC as template, PVA as an additive to reduce cracking of the films, and PAA/MPA-stabilized CdS QDs with different loading concentrations. $Si(OCH_3)_4$ was first mixed with a PVA (2 wt%)/CNC dispersion (3.0 wt% CNC, pH 2.4) with 0.23 mL $Si(OCH_3)_4$/0.15 g CNC ratio and stirred until a homogeneous mixture was obtained. Subsequently, different volumes (1.5–4.0 mL) of the PAA/MPA-stabilized CdS QD aqueous solution (5.14 mM, pH ≈ 5) were added and the homogeneous mixture was stirred for 10 min. Silica/CNC composites loaded with 1.15, 1.88, and 2.23 mM PAA/MPA-stabilized CdS QDs (concentrations reflect the initial concentration of Cd^{2+} ions used) obtained after drying in a fumehood for 48 h are denoted **CQ1**, **CQ2**, and **CQ3**, respectively (see Table S1 in Supporting Information). These three samples have calculated Cd:Si ratios of ca. 0.5:100, 1.0:100, and 1.4:100 for **CQ1**-**CQ3**, respectively.

Owing to the instability of the MPA-capped CdS QDs in acidic media, the resulting CdS/silica/CNC composites show a disruption of the chiral nematic order when a high concentration (2.23 mM) of the MPA-capped QDs was employed without PAA. In contrast, the use of PAA as a stabilizer allowed a wide range of the CdS QD concentrations to be used without the disruption of the chiral nematic order. Silica/CNC composites loaded with either low (1.15 mM) or high (2.23 mM) concentrations of the PAA/MPA-stabilized CdS QDs showed both iridescence and bright luminescence (Figure S5, Supporting Information). This indicates that the chiral nematic order of CNC and the emissive properties of the PAA/MPA-stabilized QDs were both preserved during co-assembly. The QD luminescence was unchanged even in the assembly environment at pH 2.4, which can be attributed to an efficient QD surface passivation by PAA. This could inhibit strong interactions with the CNC surface, thus preserving the chiral nematic organization of CNC. Visually, the PAA/MPA-stabilized CdS QDs were more

evenly dispersed in the silica/CNC composites in the presence of PVA, showing far fewer yellow-colored spots than when the MPA-capped QDs were used without PAA.

Varying the PAA/MPA-stabilized CdS QD concentration while fixing the silica/CNC proportion in the preparations allows complementary control of the optical properties of the composites. Polarized optical microscopy (POM) images of the CdS/silica/CNC composites show textures characteristic of a chiral nematic structure with a blue-colored shift relative to the silica/CNC composites (Figures S6a,b, Supporting Information). Scanning electron microscopy (SEM) images (Figure S7, Supporting Information) viewed along fracture edges of the CdS/silica/CNC composites show twisted layered features, demonstrating that the chiral nematic order of CNC was preserved during inclusion of the PAA/MPA-stabilized CdS QDs into the silica/CNC composites. QDs embedded within the composites were not observed by electron microscopy. This is reasonable considering their tiny particle size and the good dispersion of the PAA/MPA-stabilized CdS QDs within the composites.

The CdS/silica/CNC composites loaded with different QD concentrations appear iridescent and have the same red-colored luminescence but different brightness when viewed under UV light irradiation (**Figure 1**a and Figure S5, Supporting Information). Optical spectra (Figures 1b,c) of the composites **CQ1**, **CQ2**, and **CQ3** show an absorption edge at 405 nm and a broad PL emission peak at 680 nm both assigned to the CdS QDs; a reflectance peak at ≈600–1200 nm is characteristic of the chiral nematic structure. PL emission intensity is about proportional to the QD loading range employed; for comparison, a chiral nematic silica/CNC composite sample without QD loading (**CQ0**) is non-luminescent (Figure 1b). The emission wavelength of the CdS/silica/CNC composites red-shifted over 70 nm relative to the PAA/MPA-stabilized CdS QDs in aqueous solution. As this red-shift is nearly independent of the QD concentration, it is probably due to the effect of changing the environment of QDs (solid vs solution) rather than aggregation of QDs during co-assembly. Interestingly, the magnitude of the blue-shift in reflectance wavelength of the chiral nematic CdS/silica/CNC composites scales with the QD concentration employed in the assembly (Figure 1c). This shift is similar to what is observed with the addition of monovalent salts to the CNC dispersions, where the increased ionic strength of the dispersion leads to a blue-shift of the chiral nematic reflection peak originating from a decrease in the helical pitch.[18] Thus, the PAA/MPA-stabilized QD colloids effectively increase the ionic strength in the dispersion and affect the resulting pitch of the chiral nematic structure. Circular dichroism (CD) spectra (Figure 1d) of the CdS/silica/CNC composites show that the position of the CD peak closely matches the peak reflection wavelength, demonstrating that co-assembling the water-soluble PAA/MPA-stabilized CdS QD colloids with tetraalkoxysilane and lyotropic CNC dispersion preserved the left-handed chiral nematic order in the CdS/silica/CNC composites.

Calcination of the composites **CQ1**, **CQ2**, and **CQ3** under air to remove the cellulose template and organic stabilizers (MPA, PAA, PVA) generated mesoporous CdS/silica films **SQ1**, **SQ2**, and **SQ3**, respectively (see Table S1, Supporting Information). The usual calcination temperature for the decomposition of the cellulose from silica/CNC composites to recover mesoporous silica is 540 °C for 6 h,[10a] but we found that when the composites are calcined at >500 °C, the CdS is oxidized and its luminescence disappears (Figure S8, Supporting Information). To retain the luminescence of the CdS QDs inside the silica, the composites were calcined under air at 450 °C for 24 h to decompose the organic reactants and then at 500 °C for 30 min to release residual carbon to generate mesoporous silica-encapsulated CdS films. Thermogravimetric (TGA) analyses (Figure S9, Supporting Information) show that the organic reactants in the CdS/silica/CNC composites decomposed at ≈150–600 °C and the CdS structure in the silica was stable up to 500 °C, above which the CdS was oxidized to CdO with a slight decrease in mass of ≈4 wt%. Elemental analyses confirm that the calcined CdS/silica contains only a trace amount of carbon (≈0.04 wt%), demonstrating that the cellulose template and organic stabilizers were removed.

Inductively coupled plasma-atomic emission spectrometry (ICP-AES) confirms that the calcined films (**SQ3**) are loaded with

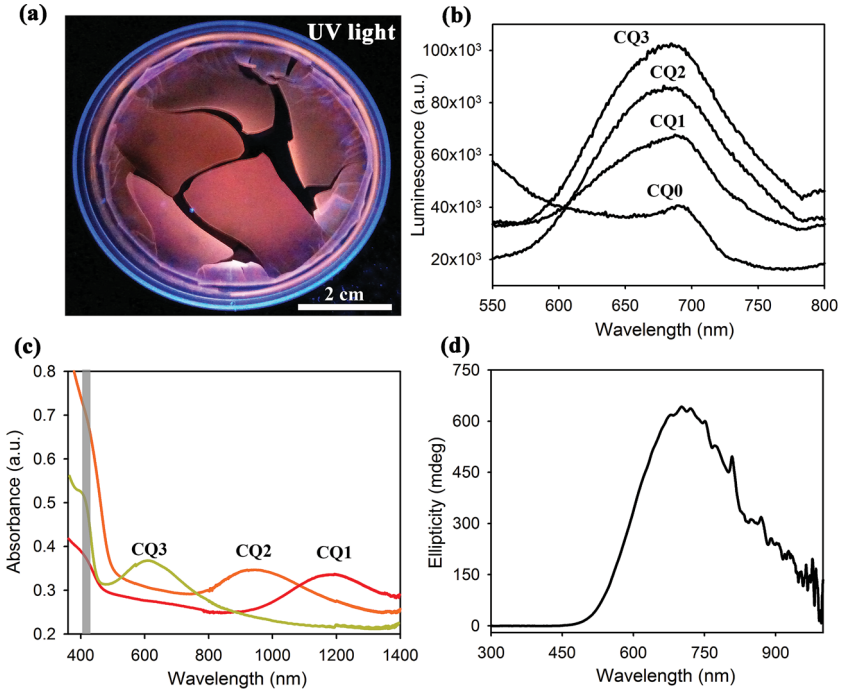

Figure 1. Co-assembly of water-soluble PAA/MPA-stabilized CdS QDs with alkoxysilane and lyotropic CNC dispersion to produce iridescent, luminescent chiral nematic CdS/silica/CNC composites. a) Photograph of the CdS/silica/CNC composites (**CQ3**) viewed under a UV lamp of wavelength 365 nm. b) Photoluminescence (PL) emission spectra (λ_{exc} = 425 nm) and c) UV-vis-NIR absorption spectra of the CdS/silica/CNC composites loaded with different QD concentrations. d) CD spectrum of **CQ3**.

0.64 wt% Cd and 0.34 wt% S corresponding to a Cd:S ratio of 1.88:1.00 and an amount of 0.69 wt% CdS loaded in **SQ3** was determined by atomic absorption spectroscopy (AAS). Energy-dispersive X-ray (EDX) spectra (Figure 3c and Figure S10a, Supporting Information) of the CdS/silica/CNC composites (**CQ3**) before and after calcination show Cd and S signals indicating the retention of these elements in these materials. The QD loading in the composites confirmed by EDX was 1.1 wt% Cd and 0.84 wt% S, while the calcined films contained 0.90 wt% Cd and 0.46 wt% S with the Cd:S ratio of 1.96:1.00. These values are higher than those determined by ICP-AES, but give a similar ratio of Cd:S and the Cd:S ratio in the composites is close to that of the pure CdS QDs. However, the sulfur component in the calcined films significantly dropped during calcination, probably due to surface oxidation of the CdS QDs inside the silica.

As expected, the calcined CdS/silica films appear iridescent combined with the light yellow color of the CdS QDs. The films show a change in iridescence from red to yellow colors with an increase in the QD loading going from **SQ1** to **SQ3** (**Figure 2**a). The luminescence of the calcined films shifted to bright green-yellow colors relative to the red-emitting composites when viewed under UV light irradiation (Figure 2b). POM images (Figure S6c, Supporting Information) of the calcined films show birefringent textures with a blue-colored shift relative to the composites. Optical spectroscopy shows the tunability of the photonic and emissive properties of the calcined films. Figure 2c shows that the CdS/silica films have a decrease in the helical pitch accompanied with a blueshift reflectance wavelength from ≈900 to ≈700 nm alongside an absorption edge at 385 nm ascribed to the CdS QDs. PL spectra (Figure 2d) of the CdS/silica films show an emission peak at 500 nm, consistent with the green-yellow luminescence observed, and the emission intensity increases as the QD loading increases from **SQ1** to **SQ3**. Unlike the CdS/silica composites, the pure iridescent mesoporous silica films (**SQ0**) show no emission at this wavelength and only a very weak peak at 695 nm typical of the chiral nematic mesoporous silica structure. It is surprising to find that the emission intensity and broadening of the PL peak of the green yellow-emitting CdS/silica films were preserved and resemble the composites. This indicates that the CdS QDs survived the calcination for the removal of the template and stabilizers. The question arises as to why the wavelength of the absorption edge and emission peak of the calcined CdS/silica films blueshifted over ≈20 nm and ≈180 nm, respectively, relative to the CdS/silica/CNC composites. This blueshift could be due to a decrease in the average particle size of the CdS QDs caused by the formation of a very thin oxidation layer around the QD surface during calcination.

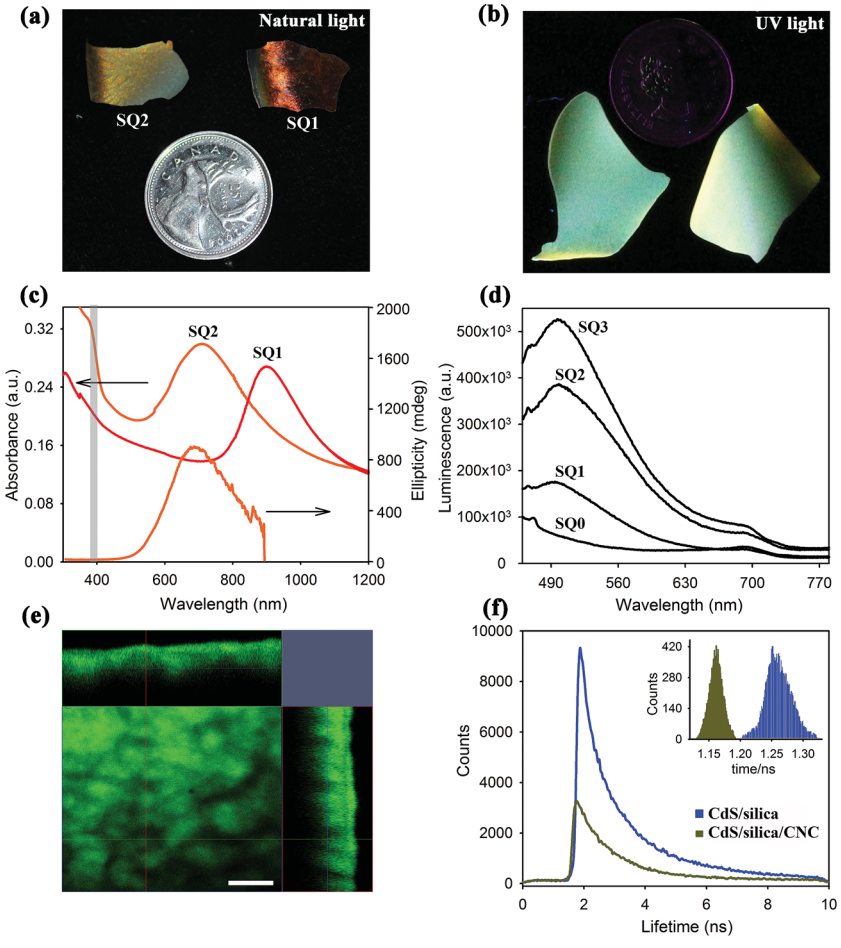

Figure 2. Iridescent, luminescent chiral nematic mesoporous silica-encapsulated CdS QD films with different QD concentrations. a) Photograph of **SQ1** and **SQ2** showing tunable red-to-yellow iridescence. b) Photograph of green yellow-emitting film (**SQ2**). c) UV-vis absorption and CD spectra of the films showing a red-to-blue shift. d) PL emission spectra of the films with different QD concentrations recorded with excitation at 425 nm. e) Confocal laser scanning luminescence image of **SQ2**, scale bar = 200 μm; the top and right images show the cross-sections of the film, while the large region shown is of the film surface. f) Lifetime decays and inset of corresponding histogram of pixel-by-pixel lifetime distributions of **CQ2** and **SQ2**.

To further investigate the emission and distribution of the CdS QDs in the silica films, confocal laser scanning luminescent microscopy and luminescence lifetime experiments

were performed. Figure 2e and Figure S11 (Supporting Information) present luminescent images of the CdS/silica/CNC composites before and after calcination in comparison with the chiral nematic mesoporous silica (**SQ0**). Luminescent *Z*-stack scanning images (Figure 2e and Figure S11b, Supporting Information) of the composites (**CQ2**) and calcined CdS/silica films (**SQ2**) show numerous analogous green luminescent dots that are invisible in the pure chiral nematic mesoporous silica (Figure S11a, Supporting Information). Expanded views of intrinsic three-dimensional luminescent images with superior penetration depth (Figure 2e and Figure S11d, Supporting Information) show bright points representative of the emission from the CdS QDs encapsulated in the silica. The luminescent domains are homogeneously dispersed throughout the films within the *x*–*y* plane as well as in the *z*-direction. These observations support the good dispersion of the luminescent CdS QDs in both the composites and calcined films.

Luminescence lifetime decays of the composites (**CQ2**) before and after calcination were measured and all fit well to a biexponential decay (Figure 2f and Supporting Information, Figure S4 and Table S2). The lifetime decay of the PAA/MPA-stabilized CdS QDs is 1.07 ± 0.01 ns in the aqueous solution.[19] After assembling QDs into the silica/CNC solid composites, the lifetime decay is 1.55 ± 0.02 ns. This value is only slightly longer than that of the CdS QDs, suggesting that the luminescence decrease by surface defect sites formed from hydrolyzed silica and CNC attaching to the QD surface is negligible,[20] and the CdS QDs are not aggregated. After calcination, the lifetime of the CdS luminescence in the mesoporous CdS/silica is 1.75 ± 0.04 ns. This result clearly demonstrates the retention of the luminescence from the CdS QDs in the silica films. The longer lifetime of the mesoporous CdS/silica can be associated with the involvement of the silica structure and surface state of the CdS QDs.[21] The porosity of the materials may allow for diffusion of air into the silica network during calcination, and the CdS QDs may anneal to induce a passivated surface through oxidation. This could be caused by a steady decrease of the surface carrier recombination processes leading to the extension of the luminescence lifetime.

The effect of the loading concentration of the CdS QDs on surface area and pores of the CdS/silica films was studied by nitrogen adsorption/desorption. **Figure 3**a shows that the CdS/silica films retain a type-IV isotherm with type-H2 hysteresis characteristic of mesoporosity. Increasing the QD loading from **SQ1** to **SQ3** resulted in a decrease in BET (Brunauer-Emmett-Teller) surface area from 590 to 450 $m^2\ g^{-1}$ and pore volume from 0.48 to 0.34 $cm^3\ g^{-1}$ for **SQ1** and **SQ3**, respectively. The BJH (Barrett-Joyner-Halenda) pore size distribution obtained from the absorption branch is about 3–6 nm and showed a slight broadening for the high CdS loading range. Both the specific surface area and pore volume both are smaller than those of the pure mesoporous silica. This difference likely results from the presence of the CdS particles that are confined inside the silica during condensation, leading to thicker pore walls. These results are consistent with the porosity changes observed for the chiral nematic mesoporous metal-stained silica films recently reported by our group.[12b]

SEM images (Figure 3b) of the mesoporous CdS/silica films show a long-range layered structure with twisted spindle-like features rotated in a counter-clockwise direction. TEM images (Figure S12, Supporting Information) of the mesoporous CdS/silica films show spindle-shaped pore networks. This reveals that the imprinted chiral nematic mesoporous structure is truly replicated from the CNC template and was preserved during incorporation of the CdS QDs into the silica. As with the composites, the CdS particles encapsulated in the silica were not observed by electron microscopy in the calcined materials. This is consistent with the small particle size of QDs and their good dispersion throughout the material. TEM images (Figure S13, Supporting Information) of CdS particles isolated by removing the silica component of the calcined films in 2 M NaOH suggest a roughly spherical shape and a mean diameter of 3 nm. This indicates that the calcination had little influence on the particle size of the as-prepared CdS QDs. The particle size and luminescence of the CdS QDs remained almost unchanged, probably due to the CdS/silica core–shell geometry encapsulated by the silica, which segregated the CdS particles and inhibited their agglomeration.

To the best of our knowledge, this is the first example of the use of the LC templating to fabricate iridescent, luminescent mesoporous materials that might be useful

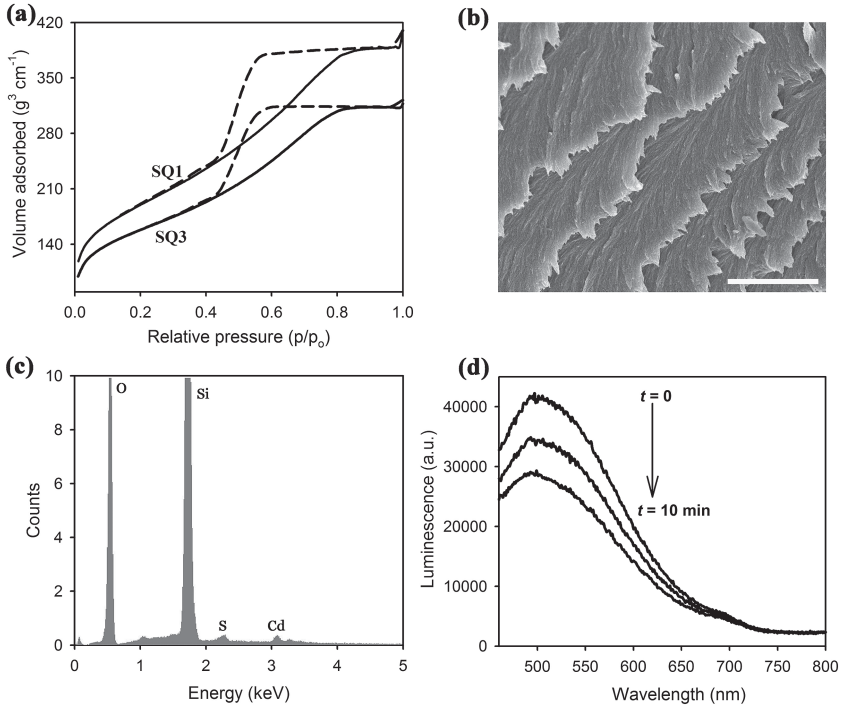

Figure 3. a) Nitrogen adsorption/desorption isotherms of chiral nematic mesoporous CdS/silica films with different QD concentrations, b) SEM image, scale bar = 2 µm, and c) EDX spectrum of **SQ3**. d) Time-dependent luminescence changes upon exposure of **SQ3** to TNT vapor.

in many possible applications.[3] Invention and design of sensitive sensors for selective detection and monitoring of trace volatile explosive threats are of great interest in counter-terrorism measures, landmine detection, and public safety.[4d,e] To demonstrate a practical application of the new CdS/silica films, we investigated the materials as optical sensors for nitroaromatic explosive 2,4,6-trinitrotoluene (TNT). Initially, we immersed a CdS/silica film (**SQ3**) in a toluene solution containing 5.5×10^{-3} mM TNT and found that its luminescence completely disappeared. The luminescence immediately returned to its original emission intensity after the film was removed from the TNT solution. The effective quenching of the luminescence originates from an electron transfer mechanism from luminescent QD donors to electron-deficient aromatic rings of TNT acceptors as observed in other systems.[22] The mesoporosity and stable solid-state structure of the CdS/silica films are important factors in determining the efficacy of these materials in reversible emission quenching and recovery.

To be useful in this application, a material must respond to vapors of the explosives. We exposed the CdS/silica films to TNT vapor and monitored the luminescence quenching; details are presented in the Supporting Information. Figure 3d depicts time-dependent luminescence quenching of the mesoporous CdS/silica films (**SQ3**) upon exposure to TNT vapor. The emission intensity gradually decreased with exposure time and reached a steady-state value after ≈10 min with quenching efficiency of 30%. This steady state value corresponds to the equilibrium established upon forming stable donor-acceptor complexes between CdS QDs and TNT.

Despite substantial recent progress in the development of efficient luminescence-based sensors for the detection of explosives,[23] porosity of the materials that allows for accessibility to the sensor components and stability of the sensing elements still remain important obstacles. Our composite materials indicate significant advantages over reported inorganic-organic hybrid composites in relation to ease of preparation and breadth of applications. Principally, the current CdS/silica composite mesoporous films i) exhibit excellent stability, ii) indicate accessibility of QDs in the gas phase and solution, and iii) require no need for binders since the materials are prepared as freestanding films. These films show promise, based on the experimental evidence presented, as new materials for the detection of explosives—needless to say, additional technical development will be necessary to improve their detection selectivity and sensitivity.

3. Conclusions

We report the first demonstration of luminescent, iridescent responses integrated into freestanding chiral nematic mesoporous silica-encapsulated CdS films. A simple one-pot approach allows rapid co-assembly of water-soluble polyacrylic acid/mercaptopropionic acid-stabilized CdS QDs with tetraalkoxysilane and lyotropic cellulose nanocrystal dispersions to give chiral nematic CdS/silica/cellulose composites. Subsequent removal of the cellulose template and other additives generated new iridescent, luminescent chiral nematic mesoporous CdS/silica films. A multi-analytical approach revealed that the CdS QDs embedded within the chiral nematic silica—after assembly and controlled calcination—are similar to those used in the initial preparation, and show no evidence of aggregation in the silica. The iridescent colors and green-yellow emission brightness of the mesoporous semiconducting photonic CdS/silica films can be tuned by changing the QD loading. The emissive films undergo luminescence quenching when exposed, for instance, to TNT solution or vapor, suggesting they could function as a selective sensory material for trace detection of TNT explosives. These new functional materials, which combine mesoporosity, chiral nematic order, and luminescence, also hold promise for developing optical nanodevices.

4. Experimental Section

Preparation of Iridescent and Luminescent Chiral Nematic Mesoporous CdS/Silica: Water-soluble MPA-capped CdS QDs were prepared through hydrothermal reaction of a homogeneous basic aqueous solution (pH ≈10) of cadmium acetate, thiourea, and MPA at 100 °C for 24 h (additional details in Supporting Information). MPA-capped CdS QDs were coated with PAA by adding 5.0 mg PAA to 17 mL of the prepared colloidal CdS QD aqueous solution under stirring at room temperature. PAA/MPA-stabilized CdS QD aqueous solution obtained was placed into a dialysis tubing and then dialyzed against distilled water for 4 h; the pH value of the colloidal solution reduced to ≈5. The resulting aqueous solution of the PAA/MPA-stabilized CdS QDs was used to prepare CdS/silica films.

Chiral nematic silica/CNC composites were prepared in a similar method as previously reported[10a] but with the addition of PVA (to reduce cracking) and PAA/MPA-stabilized CdS QDs. In a typical procedure, 20 mL of an aqueous CNC dispersion (3.0 wt%, pH 2.4) was sonicated for 10 min and then mixed with 12 mg PVA followed by 0.92 mL $Si(OCH_3)_4$ under stirring for 60 min at ambient conditions to form a homogeneous composite mixture. Different volumes (1.5–4.0 mL) of the prepared PAA/MPA-stabilized CdS QD aqueous solution (5.14 mM, pH ≈ 5) were added to portions of the $Si(OCH_3)_4$/CNC/PVA mixtures with stirring for 10 min at ambient conditions to form light yellow-colored homogeneous mixtures. The mixtures were poured into 60 mm diameter polystyrene Petri dishes and dried by water evaporation in a fumehood within 48 h to form CdS/silica/CNC composites.

Removal of the cellulose template and organic stabilizers (PAA, MPA, PVA) was performed under flowing air by heating the CdS/silica/CNC composites to 100 °C at 2 °C min^{-1}, holding at 100 °C for 2 h, heating to 450 °C at 2 °C min^{-1}, holding at 450 °C for 24 h, then heating to 500 °C at 0.5 °C min^{-1}, and holding the temperature at 500 °C for 30 min. Mesoporous CdS/silica films (SQ2) (0.15 g) were obtained from 0.30 g of the CdS/silica/CNC composites (CQ2) following the heating protocol.

Supporting Information

Supporting Information is available from the Wiley Online Library or from the author.

Acknowledgements

The authors thank CelluForce, Inc., ArboraNano, and NSERC for financial support. T.-D.N. is grateful to NSERC for a post-doctoral fellowship.

Received: July 27, 2013
Published online: October 24, 2013

[1] a) F. Marlow, Muldarisnur, P. Sharifi, R. Brinkmann, C. Mendive, *Angew. Chem. Int. Ed.* **2009**, *48*, 6212–6233; b) P. V. Braun, S. A. Rinne, F. G. Santamaria, *Adv. Mater.* **2006**, *18*, 2665–2678; c) A. Arsenault, F. Fleischhaker, G. v. Freymann, V. Kitaev, H. Miguez, A. Mihi, N. Tetreault, E. Vekris, I. Manners, S. Aitchison, D. Perovic, G. A. Ozin, *Adv. Mater.* **2006**, *18*, 2779–2785; d) E. V. Schwoob, C. Weisbuch, H. Benisty, S. Olivier, S. Varoutsis, I. R. Philip, R. Houdre, C. J. M. Smith, *Phys. Rev. Lett.* **2005**, *95*, 183901.

[2] a) A. P. Alivisatos, *Science* **1996**, *271*, 933–937; b) J. M. Bruchez, M. Moronne, P. Gin, S. Weiss, A. P. Alivisatos, *Science* **1998**, *281*, 2013–2016.

[3] a) K. Aoki, D. Guimard, M. Nishioka, M. Nomura, S. Iwamoto, Y. Arakawa, *Nat. Photonics* **2008**, *2*, 688–692; b) A. C. Arsenault, T. J. Clark, G. V. Freymann, L. Cademartiri, R. Sapienza, J. Bertolotti, E. Vekris, S. Wong, V. Kitaev, I. Mnners, R. Z. Wang, S. John, D. Wiersma, G. A. Ozin, *Nat. Mater.* **2006**, *5*, 179–184; c) O. Painter, R. K. Lee, A. Scherer, A. Yariv, J. D. O'Brien, P. D. Dapkus, I. Kim, *Science* **1999**, *284*, 1819–1821; d) S. Ogawa, M. Imada, S. Yoshimoto, M. Okano, S. Noda, *Science* **2004**, *305*, 227–229.

[4] a) I. L. Medintz, H. T. Uyeda, E. R. Goldman, H. Mattoussi, *Nat. Mater.* **2005**, *4*, 435–446; b) K. E. Sapsford, L. Berti, I. L. Medintz, *Angew. Chem. Int. Ed.* **2006**, *45*, 4562–4588; c) R. Freeman, I. Willner, *Chem. Soc. Rev.* **2012**, *41*, 4067–4085; d) M. B. Pushkarsky, I. G. Dunayevskiy, M. Prasanna, A. G. Tsekoun, R. Go, C. K. N. Patel, *Proc. Natl. Acad. Sci. U. S. A.* **2006**, *103*, 19630–19634; e) S. W. Thomas III, G. D. Joly, T. M. Swager, *Chem. Rev.* **2007**, *107*, 1339–1386.

[5] a) P. Lodah, A. F. v. Driel, I. S. Nikolaev, A. Irman, K. Overgaag, D. Vanmaekelbergh, W. L. Vos, *Nature* **2004**, *430*, 654–657; b) P. D. Garcia, A. Blanco, A. Shavel, N. Gaponik, A. Eychmüller, B. R. Gonzalez, L. M. L. Marzan, C. Lopez, *Adv. Mater.* **2006**, *18*, 2768–2772.

[6] a) A. Thomas, M. Antonietti, *Adv. Funct. Mater.* **2003**, *13*, 763–766; b) C. Sanchez, H. Arribart, M. M. G. Guille, *Nat. Mater.* **2005**, *4*, 277–288; c) S. J. Woltman, G. D. Jay, G. P. Crawford, *Nat. Mater.* **2007**, *6*, 929–938; d) W. J. Chung, J. W. Oh, K. Kwak, B. Y. Lee, J. Meyer, E. Wang, A. Hexemer, S. W. Lee, *Nature* **2011**, *478*, 364–368; e) A. Kuzyk, R. Schreiber, Z. Fan, G. Pardatscher, E. M. Roller, A. Hogele, F. C. Simmel, A. O. Govorov, T. Liedl, *Nature* **2012**, *483*, 311–314.

[7] a) S. B. Candanedo, M. Roman, D. G. Gray, *Biomacromolecules* **2005**, *6*, 1048–1054; b) W. Y. Hamad, T. Q. Hu, *Can. J. Chem. Eng.* **2010**, *88*, 392–402; c) K. Shanmuganathan, J. R. Capadona, S. J. Rowan, C. Weder, *J. Mater. Chem.* **2010**, *20*, 180–186; d) A. Walther, J. V. I. Timonen, I. Diez, A. Laukkanen, O. Ikkala, *Adv. Mater.* **2011**, *23*, 2924–2928; e) S. Beck, J. Bouchard, R. Berry, *Biomacromolecules* **2012**, *13*, 1486–1494.

[8] a) R. H. Marchessault, F. F. Morehead, N. M. Walter, *Nature* **1959**, *184*, 632–633; b) J. F. Revol, L. Godbout, D. G. Gray, *J. Pulp. Pap. Sci.* **1998**, *24*, 146–149; c) Y. Habibi, L. A. Lucia, O. J. Rojas, *Chem. Rev.* **2010**, *110*, 3479–3500; d) G. Picard, D. Simon, Y. Kadiri, J. D. LeBreux, F. Ghozayel, *Langmuir* **2012**, *28*, 14799–14807; e) J. Majoinen, E. Kontturi, O. Ikkala, D. G. Gray, *Cellulose* **2012**, *19*, 1599–1605.

[9] E. Dujardin, M. Blaseby, S. Mann, *J. Mater. Chem.* **2003**, *13*, 696–699.

[10] a) K. E. Shopsowitz, H. Qi, W. Y. Hamad, M. J. MacLachlan, *Nature* **2010**, *468*, 422–425; b) K. E. Shopsowitz, W. Y. Hamad, M. J. MacLachlan, *J. Am. Chem. Soc.* **2012**, *134*, 867–870.

[11] J. A. Kelly, M. Yu, W. Y. Hamad, M. J. MacLachlan, *Adv. Opt. Mater.* **2013**, *1*, 295–299.

[12] a) H. Qi, K. E. Shopsowitz, W. Y. Hamad, M. J. MacLachlan, *J. Am. Chem. Soc.* **2011**, *133*, 3728–3731; b) J. A. Kelly, K. E. Shopsowitz, J. M. Ahn, W. Y. Hamad, M. J. MacLachlan, *Langmuir* **2012**, *28*, 17256–17262.

[13] a) T. Abitbol, D. Gray, *Chem. Mater.* **2007**, *19*, 4270–4276; b) T. Abitbol, D. G. Gray, *Cellulose* **2009**, *16*, 319–326; c) T. Abitbol, J. T. Wilson, D. G. Gray, *J. Appl. Polym. Sci.* **2011**, *119*, 803–810.

[14] a) C. d. M. Donega, P. Liljeroth, D. Vanmaekelbergh, *Small* **2005**, *1*, 1152–1162; b) X. Wang, W. Li, B. Zhao, D. Zhang, K. Sun, X. An, Z. Zhang, Z. Shen, *RSC Adv.* **2013**, *3*, 3553–3556.

[15] a) H. Li, W. Y. Shih, W. H. Shih, *Ind. Eng. Chem. Res.* **2007**, *46*, 2013–2019; b) A. Aboulaich, D. Billaud, M. Abyan, L. Balan, J. J. Gaumet, G. Medjadhi, J. Ghanbaja, R. Schneider, *ACS Appl. Mater. Interfaces* **2012**, *4*, 2561–2569.

[16] a) C. Luccardini, C. Tribet, F. Vial, V. M. Artzner, M. Dahan, *Langmuir* **2006**, *22*, 2304–2310; b) B. A. Kairdolf, A. M. Smith, S. Nie, *J. Am. Chem. Soc.* **2008**, *130*, 12866–12867.

[17] S. Beck, J. Bouchard, G. Chauve, R. Berry, *Cellulose* **2013**, *20*, 1401–1411.

[18] a) X. M. Dong, T. Kimura, J. F. Revol, D. G. Gray, *Langmuir* **1996**, *12*, 2076–2082; b) X. M. Dong, D. G. Gray, *Langmuir* **1997**, *13*, 2404–2409; c) J. Pan, W. Hamad, S. K. Straus, *Macromolecules* **2010**, *43*, 3851–3858; d) S. Beck, J. Bouchard, R. Berry, *Biomacromolecules* **2011**, *12*, 167–172.

[19] a) P. P. Jha, P. G. Sionnest, *ACS Nano* **2009**, *3*, 1011–1015; b) S. S. L. Sobhana, M. V. Devi, T. P. Sastry, A. B. Mandal, *J. Nanopart. Res.* **2011**, *13*, 1747–1757.

[20] a) S. Dembski, C. Graf, T. Kruger, U. Gbureck, A. Ewald, A. Bock, E. Ruhl, *Small* **2008**, *4*, 1516–1526; b) R. Koole, M. M. v. Schooneveld, J. Hilhorst, C. d. M. Donega, D. C. 't Hart, A. v. Blaaderen, D. Vanmaekelbergh, A. Meijerink, *Chem. Mater.* **2008**, *20*, 2503–2512.

[21] a) X. Wang, W. Li, B. Zhao, D. Zhang, K. Sun, X. An, Z. Zhang, Z. Shen, *RSC Adv.* **2013**, *3*, 3553–3556; b) S. Jun, J. Lee, E. Jang, *ACS Nano* **2013**, *7*, 1472–1477.

[22] a) E. R. Goldman, I. L. Medintz, J. L. Whitley, A. Hayhurst, A. R. Clapp, H. T. Uyeda, J. R. Deschamps, M. E. Lassman, H. Mattoussi, *J. Am. Chem. Soc.* **2005**, *127*, 6744–6751; b) J. S. Yang, T. M. Swager, *J. Am. Chem. Soc.* **1998**, *120*, 5321–5322; c) R. Tu, B. Liu, Z. Wang, D. Gao, F. Wang, Q. Fang, Z. Zhang, *Anal. Chem.* **2008**, *80*, 3458–3465; d) K. Zhang, H. Zhou, Q. Mei, S. Wang, G. Guan, R. Liu, J. Zhang, Z. Zhang, *J. Am. Chem. Soc.* **2011**, *133*, 8424–8427; e) Y. Ma, H. Li, S. Peng, L. Wang, *Anal. Chem.* **2012**, *84*, 8415–8421.

[23] a) A. Rose, Z. Zhu, C. F. Madigan, T. M. Swager, V. Bulovic, *Nature* **2005**, *434*, 876–879; b) Y. Xia, L. Song, C. Zhu, *Anal. Chem.* **2011**, *83*, 1401–1407; c) R. Freeman, T. Finder, L. Bahshi, R. Gill, I. Willner, *Adv. Mater.* **2012**, *24*, 6416–6421; d) W. Wei, X. Huang, K. Chen, Y. Tao, X. Tang, *RSC Adv.* **2012**, *2*, 3765–3771; e) T. Pazhanivel, D. Nataraj, V. P. Devarajan, V. Mageshwari, K. Senthil, D. Soundararajan, *Anal. Methods* **2013**, *5*, 910–916; f) S. S. Nagarkar, B. Joarder, A. K. Chaudhari, S. Mukherjee, S. K. Ghosh, *Angew. Chem. Int. Ed.* **2013**, *52*, 2881–2885.